Computer Modeling in Engineering & Sciences

Tech Science Press

DOI: 10.32604/cmes.2024.053199

ARTICLE

Magneto-Photo-Thermoelastic Excitation Rotating Semiconductor Medium Based on Moisture Diffusivity

Khaled Lotfy[1,2], A. M. S. Mahdy[3,*], Alaa A. El-Bary[4] and E. S. Elidy[1]

[1]Department of Mathematics, Faculty of Science, Zagazig University, Zagazig, 44519, Egypt

[2]Department of Mathematics, Faculty of Science, Taibah University, Madinah, 42353, Saudi Arabia

[3]Department of Mathematics and Statistics, College of Science, Taif University, Taif, 11099, Saudi Arabia

[4]Arab Academy for Science, Technology and Maritime Transport, Alexandria, 1029, Egypt

*Corresponding Author: A. M. S. Mahdy. Email: amattaya@tu.edu.sa

Received: 27 April 2024 Accepted: 21 June 2024 Published: 20 August 2024

ABSTRACT

In this research, we focus on the free-surface deformation of a one-dimensional elastic semiconductor medium as a function of magnetic field and moisture diffusivity. The problem aims to analyze the interconnection between plasma and moisture diffusivity processes, as well as thermo-elastic waves. The study examines the photo-thermoelasticity transport process while considering the impact of moisture diffusivity. By employing Laplace's transformation technique, we derive the governing equations of the photo-thermo-elastic medium. These equations include the equations for carrier density, elastic waves, moisture transport, heat conduction, and constitutive relationships. Mechanical stresses, thermal conditions, and plasma boundary conditions are used to calculate the fundamental physical parameters in the Laplace domain. By employing numerical techniques, the Laplace transform is inverted to get complete time-domain solutions for the primary physical domains under study. Reference moisture, thermoelastic, and thermoelectric characteristics are employed in conjunction with a graphical analysis that takes into consideration the effects of applied forces on displacement, moisture concentration, carrier density, stress due to forces, and temperature distribution.

KEYWORDS

Moisture diffusivity; semiconductor; photothermoelastic; rotation; thermomechanical waves; laplace transform

1 Introduction

The study of how mechanical and thermal processes interact with one another in a material is known as thermoelasticity. The impact of rotation on material behavior is one of the fascinating features of thermoelasticity. In thermoelasticity, rotation is the result of mechanical or thermal forcing on a solid substance. The rotation might be calculated as part of the solution or specified, depending on the particular situation. For instance, in a thermally induced situation, the moment brought on by the non-uniform thermal strain might create a rotation because of the material's differential expansion. A torque applied to the solid body in a mechanically generated situation has the potential to spin it. The behavior of materials, especially the distributions of stress and strain, is significantly influenced by

rotation in thermoelasticity. Thermal stress, or stress resulting from a temperature differential in the material, is a key idea in this context. The thermal stress distribution of a rotating solid body varies, which may lead to non-uniform deformation and eventual collapse. The impact of rotation on natural frequencies and vibrational modes is a significant additional factor in thermoelasticity. The modes of vibration of the material vary as it rotates, potentially leading to instability or even deterioration of the material's qualities. As a result, while assessing and creating thermoelastic systems, the influence of rotation must be taken into account.

Diffusion in thermoelasticity refers to the process where mass or heat is transferred between two or more materials due to the differences in temperature and pressure between them [1]. Recently, considerable research has been conducted on the diffusion processes in thermo-elastic materials. This research has focused on understanding the mechanisms that control the diffusion process, as well as the factors that affect the rate of diffusion. One area of intense study has been the effect of defects, such as cracks, pores, and dislocations, on the diffusion process in thermo-elastic materials. Several theoretical models have been proposed to describe the diffusion process in thermo-elastic materials. For example, the Arrhenius model assumes that the rate of diffusion is exponentially dependent on temperature and that the activation energy for diffusion can be estimated based on the energy barrier that must be overcome for diffusion to occur. Another model, the Fickian model, assumes that the speed at which diffusion occurs is directly related to the difference in concentration of the substance being diffused [2]. Overall, Diffusion in thermo-elasticity has improved knowledge of mechanisms. that control the transfer of mass and heat in these materials. The study of material properties and behavior under extreme conditions, as well as the design and development of energy conversion devices, are all significantly affected by this understanding. As research in this area continues, new models and techniques will likely be developed that further enhance our understanding of this complex phenomenon. Szekeres [1,2] investigated how generalized heat transport and moisture interact. According to Gasch et al. [3], changes in temperature and moisture levels might cause more damage than actual loads. To create equations that control the behavior of coupled hygrothermoelasticity. Povstenko [4] used the thermal stresses theories to study the time-fractional telegraph equations in the context of thermoelasticity theory.

In recent years, the photothermal (PT) technique has gained recognition for analyzing the electrical and thermal properties of semiconductor materials. These materials, increasingly important in industries like sensors, solar panels, and advanced medical equipment, are essential for renewable energy production. Semiconductors possess moderate conductivity, and when light energy interacts with them, electrons and holes are stimulated, creating electronic deformations (ED). Thermoelastic deformation (TED) refers to structural alterations caused by the excitation of electrons through light impact, leading to the creation of an electron cloud exhibiting characteristics akin to plasma waves. Heat generated in this process contributes to TED. Researchers have explored innovative methods to study how semiconductor samples react to a laser beam, including sensitivity analysis using photoacoustic spectroscopy. These explorations incorporate the application of thermoelasticity theory as well as the PT theory [5,6]. To ascertain the precise values of temperature, internal displacements, thermal diffusion, and other electrical properties of nano-composite semiconductor materials, PT techniques were applied in several physical experiments [7–10]. Electronic deformation is directly related to changes in the density of free carriers, which are in turn caused by the thermal wave generated by laser or sunlight pulses within the material's internal structures [11]. In their research, Hobiny et al. [12] examined the phenomenon of PT waves in a limitless medium by utilizing a cylindrical cavity filled with semiconductor material. These topics have been explored in various studies [13,14]. Mahdy et al. [15–18] extensively investigated the concept of photo-thermoelasticity by studying

the influence of external elements like magnetic fields and rotation on the interplay of thermal-plasma-elastic waves in semiconductor materials. Wave propagation in a photo-thermoelastic semiconductor medium is studied, together with the effects of humidity, magnetic field, and rotational field.

Sur et al. [19] studied the fibre-reinforced magneto-thermoelastic medium subjected to a moving heat source and took some applications according to the thermal therapy of cancer cells. Changing a material's temperature can substantially affect its mechanical and thermal properties. Since the expanded theory of thermoelasticity has been the subject of multiple investigations, many researchers have studied the effect of the temperature gradient, which has been largely disregarded in the past [20–24]. Understanding how temperature affects material characteristics is extremely important because we cannot assume that the characteristics of a material remain constant as temperature changes [25]. Since earlier discussions on coupled and uncoupled theories did not match up with practical tests, the thermoelasticity theory was established. This issue was fixed by the novel theory of connected thermoelasticity suggested by Biot [26]. Biot [26] proposed a dynamic theory of thermoelasticity (CD theory) that utilized The Fourier law of heat. The behavior of thermal waves moving at limitless velocities was the focus of his theory. Adding a single relaxation period to the heat equation was an innovative approach introduced by Lord et al. [27]. This was expanded upon by Green et al. [28], who added two relaxation intervals to the heat conduction equation. Multiple studies [29,30] have made use of GL's proposed generalized thermoelasticity theory. The theory explores how several types of waves behave and interact within a solid medium, including heat waves, electric fields, and mechanical vibrations. Lata et al. [31] investigated the impact of multi-dual-phase-lag heat for isotropic thermoelastic medium according to a couple stress model with two temperature theory. On the other hand, Lata [32] used fractional calculus to study the magneto-thermoelastic rotating material according to GN-II theory. Marin et al. [33] applied a new model according to Some results in Moore-Gibson-Thompson thermoelasticity with biological application for skin tissue. Roy et al. [34] studied the fractional heat order for a thermoelastic medium under the impact of voids according to three-Phase-Lag thermal memory.

This problem is investigated in the context of one-dimensional thermo-elasticity, with special attention paid to the role that mechanical force and the diffusivity of moisture play in the photo-thermal transport process. An answer is found in the research, but only at the free surface of a semi-infinite semiconducting medium. Important physical quantities have analytical solutions found by applying Laplace transforms to the governing equations. Using a powerful programming language, the inversion of the transforms is carried out numerically. The study is completed by numerically and graphically computing several properties, such as normal displacement, normal force stress, moisture concentration, carrier density, and temperature distribution.

2 Basic Equations

Assume that the object being studied is rotating evenly. In such circumstances, the angular velocity can be denoted as $\underline{\Omega} = \Omega \underline{n}$, where $\underline{n}$ is a unit vector describing the axis of rotation. There are two supplementary terms added to the motion equation in the rotating reference frame:

(1) Acceleration of Coriolis's $2\underline{\Omega} \times \dot{\underline{u}}$, $\underline{u}$ is the displacement vector.

(2) Centripetal acceleration, $\underline{\Omega} \times \left(\underline{\Omega} \times \underline{\mathrm{u}}\right)$ since motion over time is the only cause.

In a problem that involves only one dimension, every variable is solely dependent on the coordinate x and time t. considered the angular velocity as $\underline{\Omega} = (0,\ \Omega,\ 0)$. On the other hand, when there is no rotation, these terms are absent in the medium.

In addition, the magnetic field must be adjusted so that $H = H_0 + h$, $\vec{H} = (0,\ H_0,\ 0)$ is the initial magnetic field and $h\,(x,\ y,\ z)$ is the magnetic field generated in a way that is aligned with the y-axis. To start our analysis, we will focus on the linearized version of electro-dynamics in which only slow-moving mediums are considered, and there is no consideration for the electric charge density. Here is an application of Maxwell's equations, which describe the behavior of electromagnetic fields [15,16]:

$$\vec{J} = curl\,\vec{h} - \varepsilon_0 \dot{\vec{E}}, \tag{1}$$

$$curl\,\vec{E} = -\mu_0 \dot{\vec{H}}, \tag{2}$$

$$\vec{E} = -\mu_0 \left(\dot{\vec{u}} \times \vec{H}\right), \tag{3}$$

$$div\,\vec{H} = 0. \tag{4}$$

In these equations, we have the magnetic permeability represented by a symbol μ_0, the electric permeability represented by a symbol ε_0, and the particle velocity of the medium represented by the symbol $\dot{\vec{u}}$. We also assume that any small effects of temperature gradients $\dot{\vec{u}}$ can be ignored. The equations are written with a dot notation to indicate differentiation to time. Additionally, we can express the components of the vector $\vec{E}$ (which is assumed to have the same direction as the current density vector $\vec{J} = (J_1,\ J_2,\ J_3)$) in terms of displacement. The components of current density are $J_x = 0$, $J_y = 0$ and $J_z = \dfrac{\partial h}{\partial x} + \mu_0 H_0 \varepsilon_0 \ddot{u}$ when eliminating the quantities $\vec{h}$ and E from Eq. (1).

A medium's magnetic intensity is a vector whose components are [15]:

$$H_x = 0,\ H_z = 0,\ H_y = H_0 + h\ (x,\ y,\ z)\,. \tag{5}$$

Let's pretend we have a homogeneous, transversely anisotropic semiconductor material with linear elastic characteristics. Here, we explore this material's behavior throughout the PT transport stage of its life cycle. We also account for the fact that moisture and plasma-thermal diffusion within the semiconductor material often coincide. In this study, the displacement vector $u\,(r_k,\ t)$, moisture concentration $m\,(r_k,\ t)$, temperature distribution $T\,(r_k,\ t)$, and carrier density distribution (intensity) $N\,(r_k,\ t)$. The following tensor representation of the equations describes how moisture diffuses in a plasma subjected to thermal-elastic waves [35–37]:

$$\frac{\partial N\,(r_i,\ t)}{\partial t} = D_E N_{,ii}\,(r_i,\ t) - \frac{N\,(r_i,\ t)}{\tau} + \kappa\ T\,(r_i,\ t), \tag{6}$$

$$\rho\ C_e \left(D_T T_{,ii}\,(r_i,\ t) + D_T^m m_{,ii}\,(r_i,\ t)\right) = \rho\ C_e \frac{\partial \mathrm{T}\,(r_i,\ t)}{\partial t} - \frac{E_g}{\tau} N\,(r_i,\ t) + \gamma_t T_0 \frac{\partial u_{i,j}\,(r_i,\ t)}{\partial t}, \tag{7}$$

$$k_m \left(D_m\, m_{,ii}\,(r_i,\ t) + D_m^T T_{,ii}\,(r_i,\ t)\right) = k_m \frac{\partial m\,(r_i,\ t)}{\partial t} - \frac{E_g}{\tau} N\,(r_i,\ t) + \gamma_m m_0 D_m \frac{\partial u_{i,\,j}\,(r_i,\ t)}{\partial t}. \tag{8}$$

In this scenario, the effects of Lorentz force and moisture diffusion are factored into the equations of motion for a plasma wave that is subject to both a rotating field and a magnetic field [15,35]:

$$\left.\begin{array}{l} \rho \left(\ddot{\vec{u}}\,(r,\ t) + \underline{\Omega} \times \left(\underline{\Omega} \times \vec{u}\right) + 2\underline{\Omega} \times \dot{\vec{u}}\right) = \\ \mu \nabla^2 \vec{u}\,(r,\ t) + (\mu + \lambda)\,\nabla \left(\nabla .\, \vec{u}\right) - \gamma \nabla \mathrm{T} - \delta_n \nabla N - \gamma_m \nabla m + \vec{F} \end{array}\right\}. \tag{9}$$

The following equation describes the displacement and strain tensor:

$$\varepsilon_{ij} = \frac{1}{2}\left(u_{i,\,j} + u_{j,\,i}\right). \tag{10}$$

The relationship between plasma temperature, displacement, stress, and moisture concentration using a tensor form can be represented as follows [37]:

$$\sigma_{ij} = C_{ijkl}\varepsilon_{kl} - \beta_{ij}\left(\alpha_t T + d_n N\right) - \beta_{ij}^{m} m, \quad i,\, j,\, k,\, l = 1,\, 2,\, 3. \tag{11}$$

The equation includes several parameters such as temperature diffusivity D_T, the diffusion coefficient of moisture represented by D_m, D_T^m and D_m^T the coupled diffusivities. The carrier diffusion coefficient is represented by D_E, and the reference moisture and moisture diffusivity are represented by symbols m_0 and k_m, respectively. The tensor C_{ijkl} representing the symmetric isothermal parameters of an elastic medium and the strain tensor is represented by ε_{kl}. The material coefficient of moisture concentration is represented β_{ij} and β_{ij}^m, respectively. The thermal activation coupling parameter that is non-zero is $\kappa = \dfrac{\partial N_0}{\partial T}\dfrac{T}{\tau}$, the equilibrium carrier concentration is denoted by N_0 [10,12], κ is disregarded when the temperature is comparatively low. However, in the majority of cases. Assuming that the thermal activation coupling parameter is not zero, we discuss the issue at hand., although it may be neglected in certain cases where the temperature is relatively low. E_g, τ, ρ, μ, λ, and T_0 are known as the energy gap, carrier lifetime, density, Lame's elastic constants, and absolute temperature. Also, $\gamma_t = (3\lambda + 2\mu)\,\alpha_T$ is the volume thermal expansion, where α_T is the linear thermal expansion coefficient, C_e is the specific heat coefficient at constant strain for a solid plate, the conductive deformation potential and valence band difference are represented by δ_n. The semiconductor's (in the form of a rod $x = \pm 1$) elastic surface boundary conditions. Because of the thermal insulation imposed by the surface boundary conditions, closed circuits, isothermal conditions, and stress loads can all be applied without interference. Since the physical variables are independent of the yz-coordinates, all studies are performed along the x-axis. The Lorentz force is represented by $\vec{F} = \mu_0\left(\vec{J} \times \vec{H}\right)$ in 1D:

$$\vec{F} = \mu_0\left(\vec{J} \times \vec{H}\right) \equiv \left(-\mu_0 H_0 \frac{\partial h}{\partial x} - \varepsilon_0 \mu_0^2 H_0^2 \frac{\partial^2 u}{\partial t^2},\ 0,\ 0\right) \equiv F_x \vec{i}. \tag{12}$$

We can define the basic physical quantities in one dimension (1D) using the following expressions [35]:

$$\frac{\partial N}{\partial t} = D_E \frac{\partial^2 N}{\partial x^2} - \frac{N}{\tau} + \kappa\, T, \tag{13}$$

$$\rho\, C_e\left(D_T \frac{\partial^2 T}{\partial x^2} + D_T^m \frac{\partial^2 m}{\partial x^2}\right) = \rho\, C_e \frac{\partial \mathrm{T}}{\partial t} - \frac{E_g}{\tau} N + \gamma_t\, T_0 \frac{\partial e}{\partial t}, \tag{14}$$

$$k_m\left(D_m \frac{\partial^2 m}{\partial x^2} + D_m^T \frac{\partial^2 T}{\partial x^2}\right) = k_m \frac{\partial m}{\partial t} - \frac{E_g}{\tau} N + \gamma_m\, m_0 D_m \frac{\partial e}{\partial t}. \tag{15}$$

The form of the motion Eq. (9) is as follows:

$$\rho\left(\frac{\partial^2 u}{\partial t^2} - \Omega^2 u\right) = (2\mu + \lambda)\,\frac{\partial^2 u}{\partial x^2} - \gamma \frac{\partial T}{\partial x} - \delta_n \frac{\partial N}{\partial x} - \gamma_m \frac{\partial m}{\partial x} - \mu_0 H_0 \frac{\partial h}{\partial x} - \varepsilon_0 \mu_0^2 H_0^2 \frac{\partial^2 u}{\partial t^2}, \tag{16}$$

where $\gamma_{t,\,m} = \beta\,\alpha_{m,\,T}$, $\delta_n = \beta d_n$, $\beta = 3\mu + 2\lambda$, and $h = -H_0 e$.

The equation that defines the relationship in one dimension can be expressed as:

$$\sigma_{xx} = (2\mu + \lambda)\frac{\partial u}{\partial x} - \beta\left(\alpha_t T + d_n N\right) - \gamma_m m = \sigma. \tag{17}$$

3 Mathematical Formulation of the Problem

To make it simpler, new simplified variables are introduced that have no units associated with them.

$$(x',\ u') = \frac{(x,\ u)}{C_T t^*},\ \Omega' = t^*\Omega,\ (T',\ N') = \frac{(\gamma_t T,\ \delta_n N)}{2\mu + \lambda},\ m' = m,\ e' = e,\ t' = \frac{t}{t^*},\ h' = \frac{h}{\rho C_T^2},\ \sigma' = \frac{\sigma}{\mu} \tag{18}$$

In Eqs. (13)–(17), the dashes are omitted for convenience. Using Eq. (18), when the strain in 1D is $e = u_x$, yields:

$$\left(\nabla^2 - \alpha_1 - \alpha_2\frac{\partial}{\partial t}\right)N + \varepsilon_3 T = 0, \tag{19}$$

$$\left(\nabla^2 - b_1\frac{\partial}{\partial t}\right)T + b_2\nabla^2 m + b_3 N - \varepsilon_1\frac{\partial e}{\partial t} = 0, \tag{20}$$

$$\left(\nabla^2 - b_4\frac{\partial}{\partial t}\right)m + b_5\nabla^2 T + b_6 N - b_7\frac{\partial e}{\partial t} = 0, \tag{21}$$

$$\left(\alpha\nabla^2 - R_H\frac{\partial^2}{\partial t^2} - \Omega^2\right)e - \nabla^2 T - \nabla^2 N - b_8\nabla^2 m = 0. \tag{22}$$

The stress component in one dimension appears in the non-dimensional form in the following way:

$$\sigma_{xx} = b_9\left(e - (T + N)\right) - b_{10} m = \sigma. \tag{23}$$

where

$$\alpha_1 = \frac{kt^*}{D_E\rho\tau C_e},\ \alpha_2 = \frac{k}{D_E\rho C_e},\ b_1 = \frac{C_T^2 t^*}{D_T},\ b_2 = \frac{D_T^m\gamma_t}{D_T(2\mu + \lambda)},\ \varepsilon_2 = \frac{\alpha_T E_g t^*}{\tau d_n\rho C_e},\ b_3 = \varepsilon_2 b_1\,\varepsilon_1 = \frac{\gamma_t^2 T_0 t^*}{k\rho},$$

$$b_4 = \frac{C_T^2 t^*}{D_m},\ b_5 = \frac{D_m^T(2\mu + \lambda)}{D_m\gamma_t},\ b_6 = \frac{E_g(2\mu + \lambda)t^* b_4}{k_m\delta_n\tau},\ b_7 = \frac{\gamma_m m_0 C_T^2 t^*}{k_m}, b_8 = \frac{\gamma_m}{2\mu + \lambda}\,\varepsilon_3 = \frac{d_n k\kappa t^*}{\alpha_T\rho C_e D_E},$$

$$b_9 = \frac{2\mu + \lambda}{\mu},\ b_{10} = \frac{\gamma_m}{\mu}\ C_T^2 = \frac{2\mu + \lambda}{\rho},\ \delta_n = (2\mu + 3\lambda)\,d_n,\ t^* = \frac{k}{\rho C_e C_T^2},\ \alpha = 1 + \mu_0 H_0^2/(2\mu + \lambda),$$

$R_H = 1 + \varepsilon_0\mu_0^2 H_0^2/\rho$.

The parameters ε_3, ε_1, and ε_2 can be called the thermoelectric coupling parameter, the thermoelastic coupling parameter, and the thermo-energy coupling parameter, respectively.

One way to approach solving an analytical problem involves taking into account certain initial conditions that exhibit homogeneity properties. These conditions can be expressed as follows:

$$\begin{aligned} &e(x,\ t)|_{t=0} = \left.\frac{\partial e(x,t)}{\partial t}\right|_{t=0} = 0,\ T(x,t)|_{t=0} = \left.\frac{\partial T(x,t)|}{\partial t}\right|_{t=0} = 0,\ m(x,t)|_{t=0} = \left.\frac{\partial m(x,t)}{\partial t}\right|_{t=0} = 0. \\ &\sigma(x,t)|_{t=0} = \left.\frac{\partial\sigma(x,t)}{\partial t}\right|_{t=0} = 0,\ N(x,t)|_{t=0} = \left.\frac{\partial N(x,t)}{\partial t}\right|_{t=0} = 0. \end{aligned} \tag{24}$$

4 The Solution to the Problem

Using Laplace transformation, which is a mathematical technique that can be utilized on any function $\Im(x,\ t)$, according to its definition:

$$L\left(\Im\left(x,\ t\right)\right)=\overline{\Im}\left(x,\ s\right)=\int_0^{\infty}\Im\left(x,\ t\right)\exp\left(-st\right)d\,t. \tag{25}$$

Using Eq. (25) for the basic five Eqs. (19)–(23), yields:

$$\left(D^2-\alpha_3\right)\overline{N}+\varepsilon_3\overline{T}=0, \tag{26}$$

$$\left(D^2-\alpha_4\right)\overline{T}+b_2D^2\overline{m}+b_3\overline{N}-\alpha_5\overline{e}=0, \tag{27}$$

$$\left(D^2-\alpha_6\right)\overline{m}+b_5D^2\overline{T}+b_6\overline{N}-\alpha_7\overline{e}=0, \tag{28}$$

$$\left(\alpha D^2-\alpha_8\right)\overline{e}-D^2\overline{T}-D^2\overline{N}-b_8D\overline{m}=0, \tag{29}$$

$$\overline{\sigma}_{xx}=b_9\left(\overline{e}-\left(\overline{T}+\overline{N}\right)\right)-b_{10}\overline{m}=\overline{\sigma}, \tag{30}$$

where $D=\dfrac{d}{dx}$, $\alpha_3=\alpha_1+\alpha_2s$, $\alpha_4=b_1s$, $\alpha_5=s\varepsilon_1$, $\alpha_6=b_4s$, $\alpha_7=b_7s$, $\alpha_8=R_Hs^2+\Omega^2$.

Eliminating $\overline{T}$, $\overline{e}$, $\overline{N}$ and $\overline{m}$ between Eqs. (26)–(29), yields:

$$\left(D^8-\Theta_1D^6+\Theta_2D^4-\Theta_3D^2-\Theta_4\right)\left\{\overline{m},\ \overline{N},\ \overline{T},\ \overline{e}\right\}\left(x,\ s\right)=0. \tag{31}$$

where

$$\left.\begin{aligned}
\Theta_1&=-\frac{1}{\left(-\alpha+\alpha b_2b_5\right)}\begin{Bmatrix}\alpha\alpha_3-\alpha b_2b_5\alpha_3+\alpha\alpha_4+\alpha_5-b_5b_8\alpha_5\\+\alpha\alpha_6-b_2\alpha_7+b_8\alpha_7+\alpha_8-b_2b_5\alpha_8\end{Bmatrix}\\
\Theta_2&=\frac{\begin{Bmatrix}-\alpha\alpha_3\alpha_4-\alpha_3\alpha_5+b_5b_8\alpha_3\alpha_5-\alpha\alpha_3\alpha_6-\alpha\alpha_4\alpha_6-\alpha_5\alpha_6\\+b_2\alpha_3\alpha_7-b_8\alpha_3\alpha_7-b_8\alpha_4\alpha_7-\alpha_3\alpha_8+b_2b_5\alpha_3\alpha_8-\\\alpha_4\alpha_8-\alpha_6\alpha_8+\alpha b_3\varepsilon_3-\alpha b_2b_7\varepsilon_3-\alpha_5\epsilon_3+b_2\alpha_7\varepsilon_3\end{Bmatrix}}{\left(-\alpha+\alpha b_2b_5\right)},\\
\Theta_3&=-\frac{\begin{Bmatrix}\alpha\alpha_3\alpha_4\alpha_6+\alpha_3\alpha_5\alpha_6+b_8\alpha_3\alpha_4\alpha_7+\alpha_3\alpha_4\alpha_8+\alpha_3\alpha_6\alpha_8+\alpha_4\alpha_6\alpha_8\\+b_7b_8\alpha_5\varepsilon_3-\alpha b_3\alpha_6\varepsilon_3+\alpha_5\alpha_6\varepsilon_3-b_3b_8\alpha_7\varepsilon_3-b_3\alpha_8\varepsilon_3+b_2b_7\alpha_8\varepsilon_3\end{Bmatrix}}{\left(-\alpha+\alpha b_2b_5\right)},\\
\Theta_4&=\frac{\left\{-\alpha_3\alpha_4\alpha_6\alpha_8+b_3\alpha_6\alpha_8\varepsilon_3\right\}}{\left(-\alpha+\alpha b_2b_5\right)}.
\end{aligned}\right\}, \tag{32}$$

Using the factorization technique, the original ordinary differential equation (ODE) (31) may be solved, as shown below:

$$\left(D^2-k_1^2\right)\left(D^2-k_2^2\right)\left(D^2-k_3^2\right)\left(D^2-k_4^2\right)\left\{\overline{T},\ \overline{e},\ \overline{N},\ \overline{m}\right\}\left(x,\ s\right)=0. \tag{33}$$

where $k_i^2\ (i=1,\ 2,\ 3,\ 4)$ stands for the potential roots in the positive actual component when $x\to\infty$. Given the problem's linearity, the solution to equation (ODE) (33) looks like this:

$$\overline{T}\left(x,\ s\right)=\sum_{i=1}^{4}D_i\left(s\right)e^{-k_ix}. \tag{34}$$

The other quantities' solutions can also be stated as:

$$\overline{N}(x,\ s) = \sum_{i=1}^{4} D_i'(s)\, e^{-k_i x} = \sum_{i=1}^{4} H_{1i} D_i(s)\, e^{-k_i x}, \tag{35}$$

$$\overline{e}(x,s) = \sum_{i=1}^{4} D_i''(s) \exp(-k_i x) = \sum_{i=1}^{4} H_{2i} D_i(s) \exp(-k_i x), \tag{36}$$

$$\overline{m}(x,s) = \sum_{i=1}^{4} D_i'''(s) \exp(-k_i x) = \sum_{i=1}^{4} H_{3i} D_i(s) \exp(-k_i x), \tag{37}$$

$$\overline{\sigma}(x,s) = \sum_{i=1}^{4} D_i^{(4)}(s) \exp(-k_i x) = \sum_{i=1}^{4} H_{4i} D_i(s) \exp(-k_i x). \tag{38}$$

where D_i, D_i', D_i'', and $D_i'', i = 1, 2, 3, 4$ vary depending on the parameter and are unknown parameters s. The connection among the unknown parameters D_i, D_i', D_i'', and D_i''' can be obtained When utilizing the primary formulas (26)–(30), which describe the subsequent correlation:

$$H_{1i} = \frac{-\varepsilon_3}{m_i{}^2 - \alpha_3},$$

$$H_{2i} = \frac{\left(b_2\left(b_7 + b_3 b_8\right) k_i^2 - b_2^2 k_i^4 + \left(k_i^2 - \alpha_4\right)\left(-b_7 b_8 + k_i^2 - \alpha_6\right) + b_3\left(-k_i^2 + \alpha_6\right)\right)}{\left(k_i^2\left(\alpha_5\left(-b_7 b_8 + k_i^2 - \alpha_6\right) + b_2\left(-k_i^2\alpha_7 + b_7\left(\alpha k_i^2 - \alpha_8\right)\right)\right) + b_3\left(\alpha_6\alpha\left(aak_i^2 - \alpha_8\right) + k_i^2\left(-\alpha k_1^2 + b_8\alpha_7 + \alpha_8\right)\right)\right)},$$

$$H_{3i} = \frac{-\left(\left(-b_3 k_i^2 + k_i^2\left(k_i^2 - \alpha_4\right)\right)\left(b_7 k_i\alpha_5 - b_3 k_i\alpha_7\right) - \left(b_2 b_3 k_i^2 - b_7\left(k_i^2 - \alpha_4\right)\right)\left(-k_i^3\alpha_5 + b_3 k_2\left(\alpha k_i^2 - \alpha_8\right)\right)\right)}{\left(\left(-b_3 b_8 k_i^2 + b_2 k_i^4\right)\left(b_7 k_i\alpha_5 - b_3 k_i\alpha_7\right) - \left(-b_2 b_7 k_i^2 + b_3\left(k_i^2 - \alpha_6\right)\right)\left(-k_i^3\alpha_5 + b_3 k_i\left(\alpha k_i^2 - \alpha_8\right)\right)\right)},$$

$$H_{4i} = b_9\left(H_{2i} - (1 + H_{1i})\right) - b_{10} H_{3i}.$$

In the domain of unknown parameters $D_i(s)$, the preceding equations provide us a solution for Laplace's main variable transform. The boundary conditions will provide us these values.

5 Boundary Conditions

To specify $D_i(s)$, consider the following example: an elastic semiconductor material's outer surface is exposed to various mechanical, plasma, and thermal stresses. In every scenario, the Laplace transforms are employed:

(I) When $x = 0$, a system is thermally isolated, the free surface experiences thermal shock and serves as the isothermal boundary condition:

$$\overline{T}(0,\ s) = T_0. \tag{39}$$

Therefore,

$$\sum_{n=1}^{4} D_i(s) = \frac{T_0}{s}. \tag{40}$$

(II) To evaluate the condition of the mechanical normal stress components on the surface when $x = 0$, Laplace transformation is used:

$$\overline{\sigma}_{xx}(0,\ s) = 0. \tag{41}$$

Therefore,

$$\sum_{i=1}^{4} \{b_9 (H_{2i} - (1 + H_{1i})) - b_{10} H_{3i}\} (D_i) = 0. \tag{42}$$

(III) When the diffusion of carrier density and the photo-generation during recombination processes are being transported, the plasma boundary condition at the free surface ($x = 0$) can be expressed differently by using the Laplace transform. Here, the plasma condition takes the form of the following:

$$\overline{N} (0, s) = \frac{\lambda}{D_e} \overline{R} (s) . \tag{43}$$

In contrast, we found the following relationship:

$$\sum_{i=1}^{4} H_{1i} D_i (x, s) = \frac{\lambda}{s D_E}. \tag{44}$$

(IV) Free-surface boundary conditions for displacement when $x = 0$.

$$\overline{u} (0, s) = 0. \tag{45}$$

alternatively, the following relationship was derived:

$$\sum_{i=1}^{4} \frac{H_{2i}}{k_i} D_i (x, s) = 0. \tag{46}$$

The equations above use symbols $h(t)$ $Z(s)$ $R(s)$ that indicate the Heaviside unit step function, with a chosen constant λ. We can obtain the unknown parameters D_i via resolving these equations using the parameters.

6 Transforming the Fourier-Laplace Transforms in Reverse

Laplace transform inversion can be used to derive the dimensionally-free physical fields in the time domain. To get an approximate estimate of the Laplace transform, one can use numerical approaches like the Riemann-sum approximation method [38]. Any function $\overline{\Im} (x, s)$ in the Laplace domain may be derived as follows:

$$\Im (x, t') = L^{-1} \left\{\overline{\Im} (x, s)\right\} = \frac{1}{2\pi i} \int_{n-i\infty}^{n+i\infty} \exp (st') \overline{\Im} (x, s) \, ds. \tag{47}$$

In the case of $s = n + i\mathrm{M}$ (n, $\mathrm{M} \in R$), then the inverted Eq. (47) can be rewritten as:

$$\Im (x, t') = \frac{\exp (nt')}{2\pi} \int_{-\infty}^{\infty} \exp (i\beta t) \Im (x, n + i\beta) \, d\beta. \tag{48}$$

Extending the function over a closed interval $[0, 2t']$ with the Fourier series yields the following formula $\Im (x, t')$:

$$\Im (x, t') = \frac{e^{nt'}}{t'} \left[\frac{1}{2} \overline{\Im} (x, n) + Re \sum_{k=1}^{N} \overline{\Im} \left(x, n + \frac{ik\pi}{t'}\right) (-1)^n\right]. \tag{49}$$

where *Re* and *i* represent the real part and the imaginary unit, respectively, in this case, the sufficient N can be chosen free as a large integer but can be selected in the notation $nt' \approx 4.7$ [38].

7 Numerical Results and Discussions

The physical quantities in this problem such as displacement, temperature, moisture concentration, stress distribution, and carrier density are represented by numerical values for a brief duration. Materials are utilized for numerical simulations and SI units and constants are utilized, with software such as MATLAB used to plot the physical constants. Table 1 provides the physical constants of the semiconductor media for Si and Ge, as indicated in references [39–42].

Table 1: Material constants for Ge and Si

Name (unit)	Symbol	Ge	Si
Absolute temperature (K)	T_0	723	800
Density (kg/m^3)	ρ	5300	2330
Lamé's constants (N/m^2)	λ, μ	0.48×10^{11}, 0.53×10^{11}	6.4×10^{10}, 6.5×10^{10}
The energy gap (eV)	E_g	0.72	1.11
The coefficient of linear thermal expansion (K^{-1})	α_t	3.4×10^{-3}	4.14×10^{-6}
The coefficient of electronic deformation (m^3)	d_n	-6×10^{-31}	-9×10^{-31}
The thermal conductivity of the sample (Wm^{-1}K^{-1})	k	60	150
The carrier lifetime created by photos (s)	τ	1.4×10^{-6}	5×10^{-5}
The diffusion coefficient of carriers (m^2/s)	D_E	10^{-2}	2.5×10^{-3}
Particular heat under continuous stress (J/(kg K))	C_e	310	695
The speeds of recombination (m/s)	s	2	
The diffusion constants of moisture (m^{2}s^{-1})	D_m	0.35×10^{-2}	
Reference moisture	m_0	10%	
Coupled diffusivities $\left(\text{m}^2\,(\%\text{H}_2\text{O})/\text{s(K)}\right)$, $\left(\text{m}^2\text{s}\,(\text{K})/(\%\text{H}_2\text{O})\right)$	D_T^m D_m^T	2.1×10^{-7} 0.648×10^{-6}	
Moisture diffusivity (kg/msM)	k_m	2.2×10^{-8}	
Temperature diffusivity	D_T	$\frac{k}{\rho C_e}$	
Thermodiffusion constant of moisture (cm/cm (%H$_2$O))	α_m	2.68×10^{-3}	

7.1 The Impact of Thermoelastic Coupling Characteristics

According to the principles of photo-thermoelasticity, the representation of physical fields concerning horizontal distance (x) is shown in the first group in Fig. 1. This depiction incorporates the impact of magnetic and rotational fields on moisture diffusivity. The calculations are based on moisture diffusivity for (Si) material, and three examples of the thermoelastic coupling parameter are presented throughout all figures. The red line (____) represents $\varepsilon_1 = 0.001$, the blue line (.....) represents $\varepsilon_1 = 0.002$, and the green line (_ _ _ _) represents $\varepsilon_1 = 0.003$. In the realm of thermoelastic coupling, Fig. 1a illustrates the spatial variation of thermodynamic temperature. To ensure thermal insulation, a minimum positive temperature is necessary. Initially, temperature rises rapidly, eventually plateauing near the surface due to photo-excitation and moisture diffusion. In the subsequent phase, temperature declines to a minimum at a short distance from the surface. Fig. 1b depicts carrier density across varying distances, influenced directly by thermoelastic coupling parameters, maintaining consistency. Fig. 1c illustrates displacement distribution on a rough surface, affected by moisture diffusivity and photothermal excitation, exhibiting an increase towards the surface followed by an exponential decrease. In Fig. 1d, strain distribution due to moisture diffusivity and photo-thermal extinction unfolds, starting positively, peaking negatively, then exponentially declining to zero across different thermoelastic parameter values. Fig. 1e showcases the augmentation of stress force intensity and thermoelastic coupling parameters by mechanical stresses. Lastly, Fig. 1f presents the horizontal distribution of moisture concentration. All three cases have positive moisture concentrations. For the case when $\varepsilon_1 = 0.001$ the distribution takes a smooth reducing exponential behavior. However, when $\varepsilon_1 = 0.002$ and $\varepsilon_1 = 0.003$. The distribution experiences a significant decrease initially, followed by due to the dispersion of moisture, an exponential spread until it approaches a minimum point near to zero [43,44].

7.2 The Effect of the Thermoelectric Coupling Parameter

According to the photo-thermoelasticity theory, Fig. 2 displays the main physical fields in connection to the horizontal distance (x), including moisture diffusivity, magnetic fields, and rotational fields. The moisture diffusivity is taken into account during all calculations. when $H_0 = 10^5$ and $\mathrm{m}_0 = 10\%$ for (Si) material. Three different thermoelectric coupling parameter situations are examined in each of the subfigures. The red line (____) represents $\varepsilon_3 = -7.23 \times 10^{-36}$ the blue line (.....) expresses $\varepsilon_3 = -8.23 \times 10^{-36}$ and the green line (_ _ _ _) shows $\varepsilon_3 = -9.23 \times 10^{-36}$. Altering the dimensionless thermoelectric coupling configurations leads to distinct temperature distributions at varying distances, depicted in Fig. 2a. Initially, temperatures begin at a modest positive level, meeting the criterion for thermal insulation. Subsequently, they swiftly ascend within the first range, peaking near the surface due to photo-excitation and moisture diffusivity. In the succeeding range, temperatures diminish to a minimum well beneath the surface. Fig. 2b illustration demonstrates how carrier density evolves with distance under different thermoelastic parameters. Nevertheless, slight adjustments in thermoelectric coupling parameters have negligible effects on carrier density, which displays consistent behavior. Fig. 2c depiction showcases the horizontal displacement distribution induced by moisture diffusivity and the thermal effects of PT stimulation on a rugged surface. Starting at 0, displacement increases to maximum values close to the surface for all three thermoelectric coupling parameter cases. After then, it drops sharply till it almost reaches zero. The strain distribution with respect to horizontal distance is depicted in Fig. 2d, which is impacted by moisture diffusivity and the thermal consequences of PT stimulation on a rough surface. Commencing from a positive value, strain gradually diminishes to nearly zero levels at the surface across all three scenarios of thermoelectric coupling parameters. The amplitude of the rising stress force brought on by mechanical stresses is depicted in Fig. 2e.

Higher thermoelectric coupling parameter values tend to increase this force. Fig. 2f displays the distribution of moisture content for horizontal distance. Within the first range, the concentration drops off dramatically before growing exponentially and eventually reaching a low value close to the zero line. The main factor affecting this behavior is moisture diffusivity.

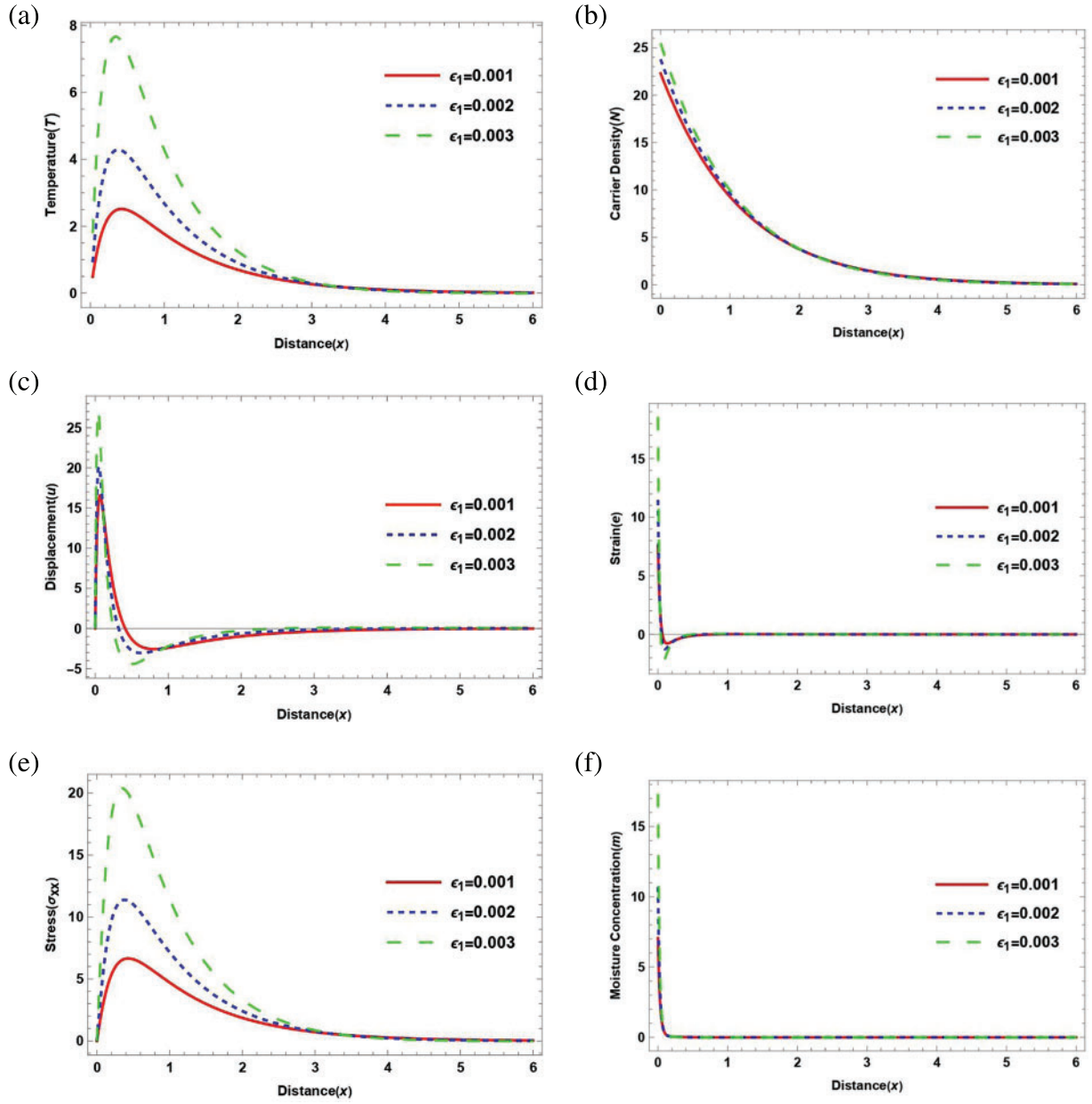

Figure 1: The variation of physical field distributions with distance with the effect of thermoelastic coupling parameter ε_1 under the effect of magnetic field $H_0 = 10^5$ and $\Omega = 5$

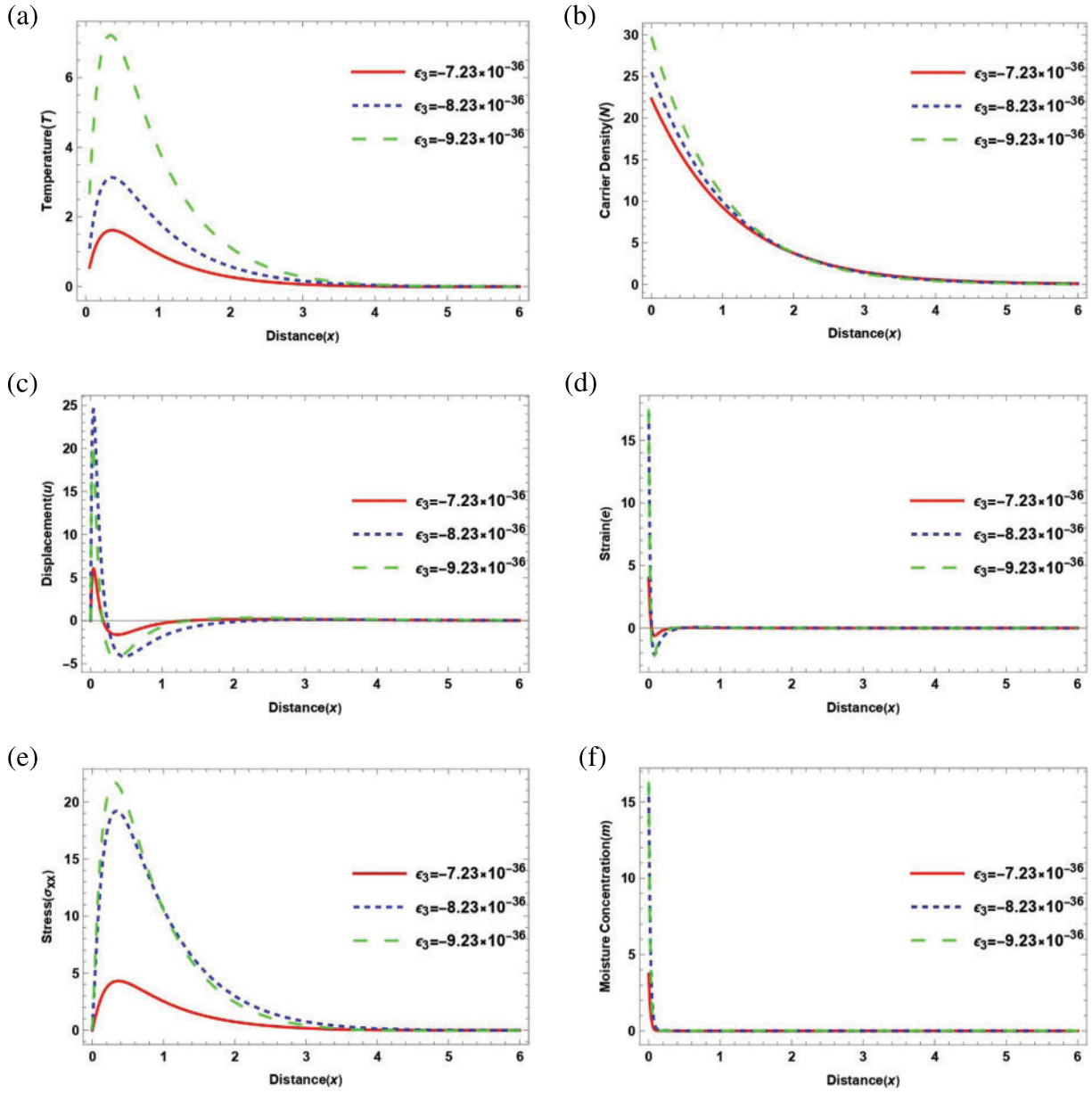

Figure 2: The variation of physical field distributions with distance at different values thermo-electric coupling parameter ε_3 under the effect of magnetic field $H_0 = 10^5$ and $\varepsilon_1 = 0.001$

7.3 Influence of Rotational Filed

Fig. 3 illustrates the relationship between the horizontal distance and the main physical fields in the third category. It showcases different values of rotational field constants, taking into account the influence of magnetic and moisture diffusivity. All calculations are conducted within the framework of thermally induced mechanical deformations. $\varepsilon_1 = 0.001$, $\varepsilon_3 = -7.23 \times 10^{-36}$, and magnetic field $H_0 = 10^5$ for (Si) material. Fig. 3 illustrates how the physical fields change concerning distance x for three different scenarios of constant rotational field. The first represents the case of rotational

felid when $\Omega = 0$ (without rotational field) (____), the second case of rotational felid when $\Omega = 0.2$ (.....), and the third case of rotational felid when $\Omega = 0.4$ (_ _ _ _). This category depicts how the rotational field has a significant impact on the propagation of displacement, strain distribution, stress force, temperature distribution, moisture concentration, and carrier density distribution [45].

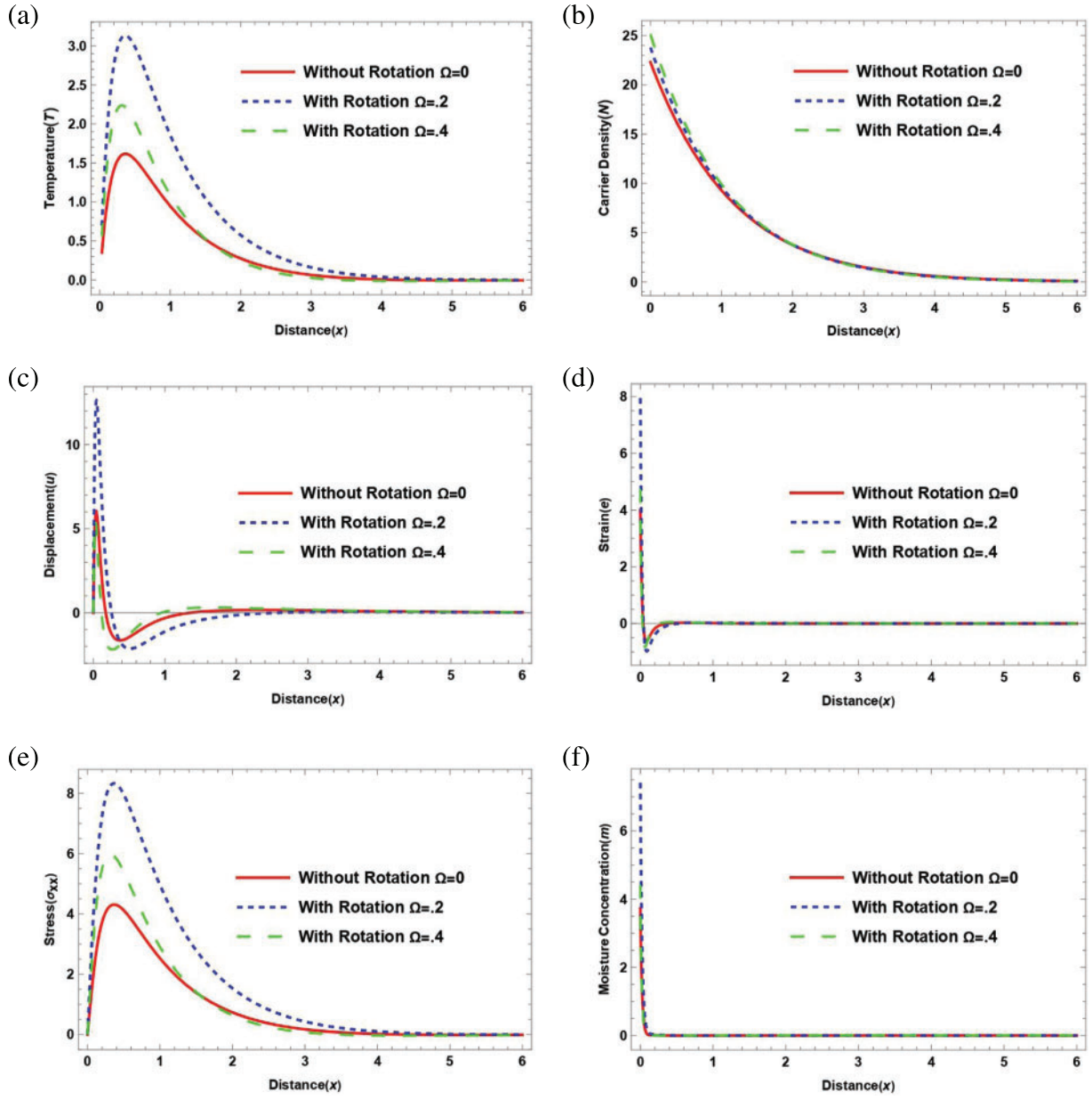

Figure 3: The variation of physical field distributions with distance with the effect of rotational field when $\varepsilon_1 = 0.001$

7.4 Influence of Reference Moisture

Fig. 4 displays the primary physical fields plotted against the horizontal distance. It depicts the variations in moisture constant along with the influence of magnetic and rotational fields in different scenarios. Thermal and elastic coupling are taken into account when conducting all calculations $\varepsilon_1 = 0.001$, $\varepsilon_3 = -7.23 \times 10^{-36}$ for Silicon (Si) material. Fig. 4 exhibits the variation of the physical fields relative to the distance in three cases of reference moisture m_0. The first when $m_0 = 10\%$ (____), the second when $m_0 = 20\%$ (.....) and the third when $m_0 = 30\%$ (_ _ _ _). This category provides evidence that the presence of moisture affects the distributions of temperature, carrier density, stress force, displacement, strain, and moisture concentration as well as how waves propagate.

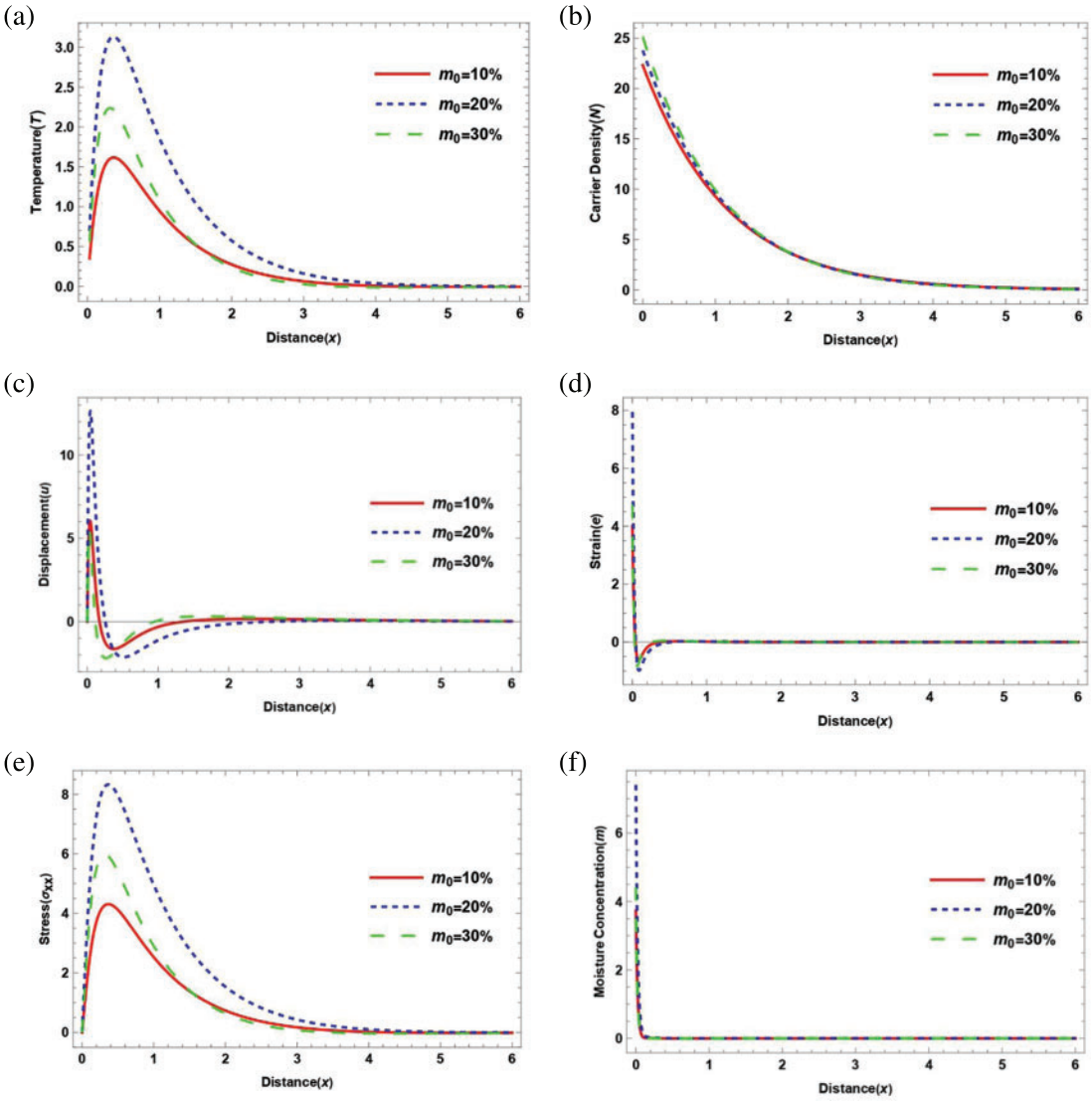

Figure 4: Shows how physical field distributions vary at different distances. The steady state of moisture m_0 under the effect of magnetic field $H_0 = 10^5$ when $\varepsilon_1 = 0.001$

7.5 Influence of Magnetic Field

The basic physical fields are displayed against a horizontal distance x in Fig. 5, together with various values of the magnetic felid constant and the influence of moisture diffusivity and the rotational field. Every computation is run using thermoelastic couples. $\varepsilon_1 = 0.001$, $\varepsilon_3 = -7.23 \times 10^{-36}$, and magnetic field $\Omega = 5$ for Silicon (Si) material. The fluctuation of the physical fields with respect to distance is shown in three situations of magnetic field constant H_0 in Fig. 5. The first represents the case of the magnetic field when $H_{0.0} = 0$ (without magnetic field) (____), the second case of the magnetic field when $H_{0.0} = 10^5$ (.....), and the third case of the magnetic field when $H_{0.0} = 5 \times 10^5$ (_ _ _ _). The given information indicates that the magnetic field has an impact on various aspects such as the movement of waves, the concentration of moisture, the force of stress, the distribution of temperature, the distribution of strain, and the density of carriers.

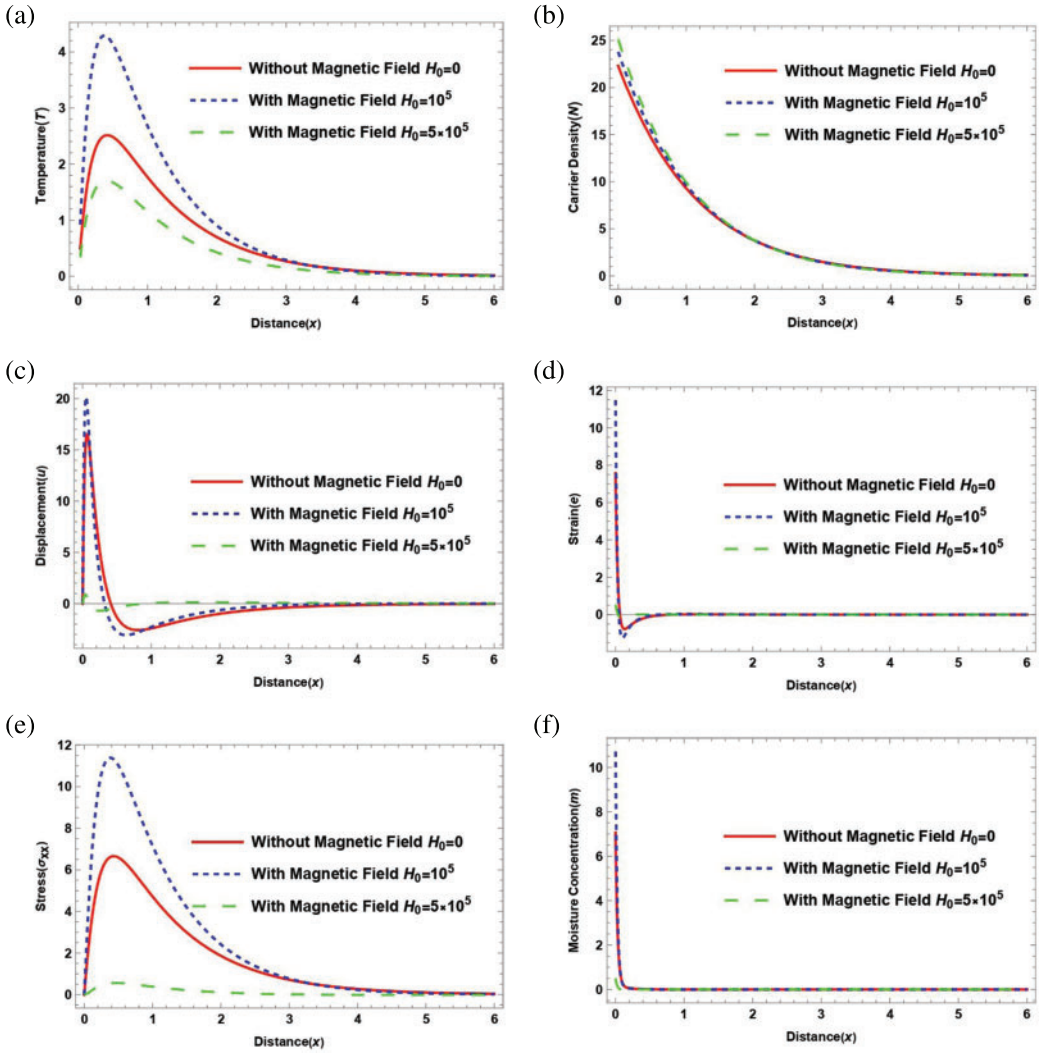

Figure 5: The variation of physical fields distribution under the effect of magnetic field H_0 when $\varepsilon_1 = 0.001$ and $\varepsilon_3 = -7 \times 10^{-36}$

7.6 The Comparison between Ge and Si Materials

Comparison of the elastic semiconductor materials (Si) and (Ge) is shown in Fig. 6. The values of the physical fields under inquiry have been numerically analyzed in this category. when $\varepsilon_1 = 0.001$ and $\varepsilon_3 = -7.23 \times 10^{-36}$ under the impact of moisture field when $m_0 = 10\%$, magnetic field $H_0 = 10^5$, and rotational field $\Omega = 5$. The given diagram clearly illustrates that there is a significant contrast in the physical constants of Ge and Si materials, which greatly impact the wave propagation across dimensionless distributions for T, e, u, σ, m and N.

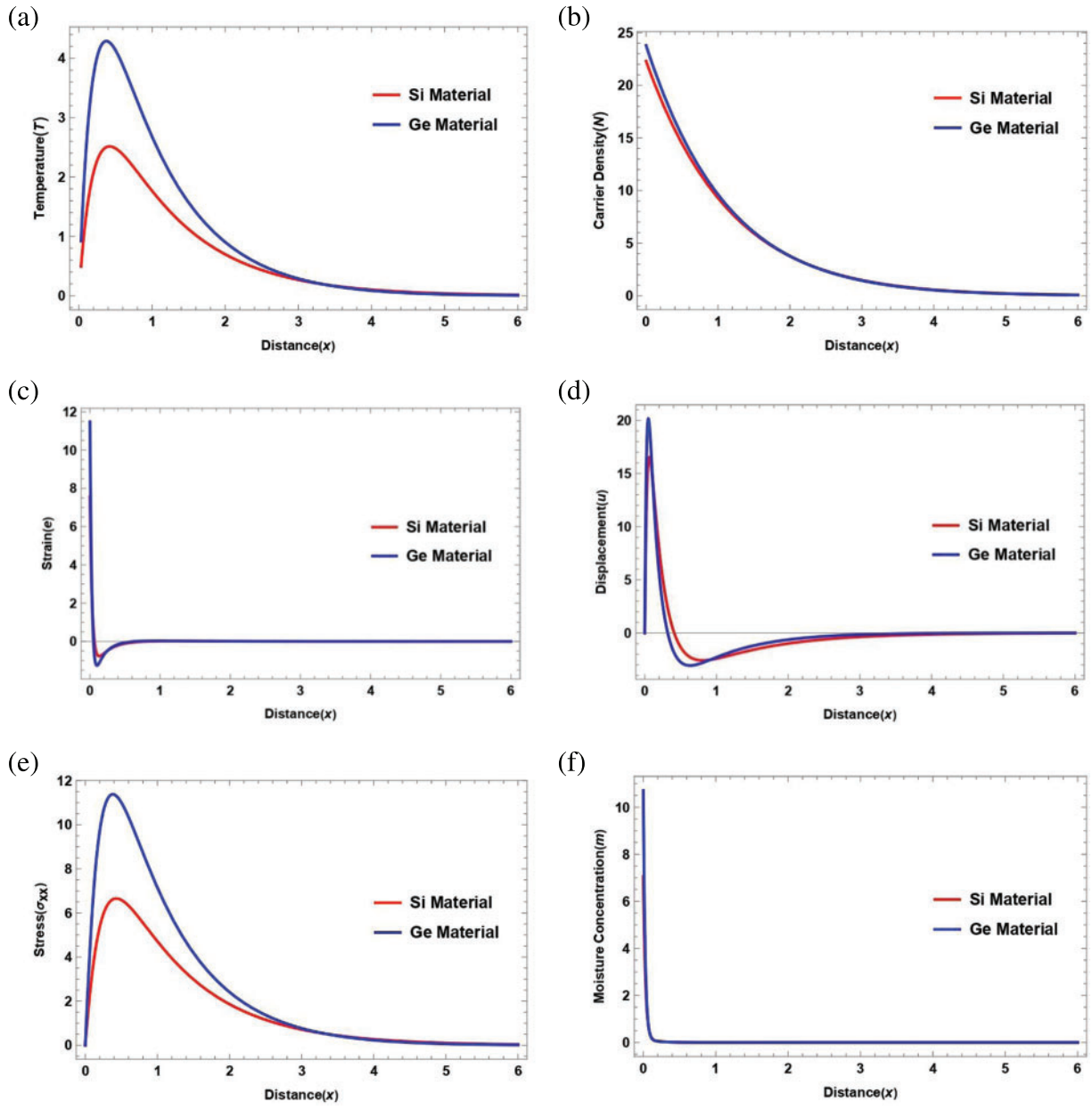

Figure 6: The comparison of physical field distributions with distance under the influence of a magnetic field in Si and Ge materials $H_0 = 10^5$ when $\varepsilon_1 = 0.001$

8 Conclusion

This study investigates how various factors influence the transmission of PT-elastic waves in solid semiconductors, particularly focusing on the impact of electron deformation on the material's deformation potential and wave generation. Using photo-thermoelasticity theory, the research analyzes wave dynamics in semiconductor media, exploring the effects of thermoelasticity, thermoelectricity, magnetic and rotational fields, and moisture concentration on wave propagation. The practical significance of photothermal theory lies in understanding material deexcitation and light absorption. The findings highlight the significant influence of medium properties on the studied aspects, benefiting physicists, material designers, thermal engineers, and geophysicists. The methodology developed offers a tool for addressing various photo-thermoelasticity and thermodynamic challenges. Understanding diffusion phenomena in thermoelasticity has wide implications in engineering, materials science, and biology. Further research in this area promises enhanced comprehension and practical applications. Additionally, studying rotational effects in thermoelasticity is crucial across industries like aerospace, energy, and biomechanics, offering safer solutions to real-world problems.

Acknowledgement: The authors extend their appreciation to Taif University, Saudi Arabia, for supporting this work through Project Number (TU-DSPP-2024-172).

Funding Statement: This research was funded by Taif University, Taif, Saudi Arabia (TU-DSPP-2024-172).

Author Contributions: Khaled Lotfy and A. M. S. Mahdy: Conceptualization, Methodology, Software. E. S. Elidy: Writing—Original draft preparation, Data curation. A. M. S. Mahdy and Alaa A. El-Bary: Supervision, Visualization, Investigation, Software, Validation. All authors: Writing—reviewing and editing. All authors reviewed the results and approved the final version of the manuscript.

Availability of Data and Materials: The data supporting this article are available upon request.

Conflicts of Interest: The study, writing, and publishing of this paper were all done without any possible conflicts of interest disclosed by the authors.

References

1. Szekeres A. Analogy between heat and moisture thermohygro-mechanical tailoring of composites by taking into account the second sound phenomenon. Compute Struct. 2000;76:145–52.
2. Szekeres A. Cross-coupled heat and moisture transport: part 1 theory. J Therm Stress. 2012;35:248–68. doi:10.1080/01495739.2012.637827.
3. Gasch T, Malm R, Ansell A. Coupled hygro-thermomechanical model for concrete subjected to variable environmental conditions. Int J Solid Struct. 2016;91:143–56. doi:10.1016/j.ijsolstr.2016.03.004.
4. Povstenko Y. Theories of thermal stresses based on space-time-fractional telegraph equations. Comput Math Appl. 2012;64(10):3321–8. doi:10.1016/j.camwa.2012.01.066.
5. Gordon JP, Leite RCC, Moore RS, Porto SPS, Whinnery JR. Long-transient effects in lasers with inserted liquid samples. Bull Am Phys Soc. 1964;119:501.
6. Kreuzer LB. Ultralow gas concentration infrared absorption spectroscopy. J Appl Phys. 1971;42:2934. doi:10.1063/1.1660651.
7. Tam AC. Ultrasensitive laser spectroscopy. New York: Academic Press; 1983. p. 1–108.

8. Tam AC. Applications of photoacoustic sensing techniques. Rev Mod Phys. 1986;58:381. doi:10.1103/RevModPhys.58.381.
9. Tam AC. Photothermal investigations in solids and fluids. Boston: Academic Press; 1989. p. 1–33.
10. Todorovic DM, Nikolic PM, Bojicic AI. Photoacoustic frequency transmission technique: electronic deformation mechanism in semiconductors. J Appl Phys. 1999;85:7716. doi:10.1063/1.370576.
11. Song YQ, Todorovic DM, Cretin B, Vairac P. Study on the generalized thermoelastic vibration of the optically excited semiconducting microcantilevers. Int J Sol Struct. 2010;47:1871–5. doi:10.1016/j.ijsolstr.2010.03.020.
12. Hobiny A, Abbas IA. A study on photothermal waves in an unbounded semiconductor medium with cylindrical cavity, mech. Time-Depend Mater. 2016;6:1–12.
13. Marin M. On existence and uniqueness in thermoelasticity of micropolar bodies. Compt Rendus de l'Acad Sci Paris, Sér II. 1995;321(12):475–80.
14. Lotfy KH. Photothermal waves for two temperature with a semiconducting medium under using a dual-phase-lag model and hydrostatic initial stress, Waves Ran. Comp Med. 2017;27(3):482–501.
15. Mahdy A, Lotfy KH, El-Bary A, Sarhan H. Effect of rotation and magnetic field on a numerical-refined heat conduction in a semiconductor medium during photo-excitation processes. Eur Phys J Plus. 2021;136: 1–17.
16. Abo-Dahab S, Lotfy KH, Gohaly A. Rotation and magnetic field effect on surface waves propagation in an elastic layer lying over a generalized thermoelastic diffusive half-space with imperfect boundary. Math Prob Eng. 2015;2015:1–15.
17. Lotfy KH, Kumar R, Hassan W, Gabr M. Thermomagnetic effect with microtemperature in a semiconducting Photothermal excitation medium. Appl Math Mech Engl Ed. 2018;39(6):783–96. doi:10.1007/s10483-018-2339-9.
18. Lotfy KH, El-Bary A, El-Sharif A. Ramp-type heating microtemperature for a rotator semiconducting material during photo-excited processes with magnetic field. Results Phys. 2020;19:103338. doi:10.1016/j.rinp.2020.103338.
19. Sur A, Kanoria M. Modeling of fibre-reinforced magneto-thermoelastic plate with heat sources. Proc Eng. 2017;173:875–82. doi:10.1016/j.proeng.2016.12.131.
20. Shakeriaski F, Ghodrat M, Escobedo-Diaz J, Behnia M. Recent advances in generalized thermoelasticity theory and the modified models: a review. J Comput Design Eng. 2021;8(1):15–35. doi:10.1093/jcde/qwaa082.
21. Hasselman D, Heller R. Thermal stresses in severe environments. New York, USA: Plenum Press; 1980.
22. Zlatić M, Čanađija M. Incompressible rubber thermoelasticity: a neural network approach. Comput Mech. 2023;71:895–916. doi:10.1007/s00466-023-02278-y.
23. Youssef H, El-Bary A. Thermal shock problem of a generalized thermoelastic layered composite material with variable thermal conductivity. Math Prob Eng. 2006;2006:87940. doi:10.1155/mpe.v2006.1.
24. Youssef H, Abbas I. Thermal shock problem of generalized thermoelasticity for an infinitely long annular cylinder with variable thermal conductivity. Comput Methods Sci Technol. 2007;13(2):95–100. doi:10.12921/cmst.
25. Marin M. An evolutionary equation in thermoelasticity of dipolar bodies. J Math Phys. 1999;40(3):1391–9. doi:10.1063/1.532809.
26. Biot MA. Thermoelasticity and irreversible thermodynamics. J Appl Phys. 1956;27:240–53. doi:10.1063/1.1722351.
27. Lord H, Shulman Y. A generalized dynamical theory of thermoelasticity. J Mech Phys Solids. 1967;15: 299–309. doi:10.1016/0022-5096(67)90024-5.
28. Green AE, Lindsay KA. Thermoelasticity. J Elast. 1972;2:1–7. doi:10.1007/BF00045689.

29. Chandrasekharaiah DS. Thermoelasticity with second sound: a review. Appl Mech Rev. 1986;39:355–76. doi:10.1115/1.3143705.
30. Hosseini SM, Sladek J, Sladek V. Application of meshless local integral equations to two dimensional analysis of coupled non-Fick diffusion-elasticity. Eng Anal Boundary Elem. 2014;37(3):603–15.
31. Lata P, Kaur H. Deformation in a homogeneous isotropic thermoelastic solid with multi-dual-phase-lag heat & two temperature using modified couple stress theory. Compos Mater Eng. 2021;3(2):89–106.
32. Lata P. Fractional effect in an orthotropic magneto-thermoelastic rotating solid of type GN-II due to normal force. Struct Eng Mech. 2022;81(4):503–11.
33. Marin M, Öchsner A, Bhatti M. Some results in Moore-Gibson-Thompson thermoelasticity of dipolar bodies, (ZAMM) Zfur Angew. Math Mech. 2020;100(12):e202000090.
34. Roy S, Lahiri A. Fractional order thermoelastic model with voids in three-phase-lag thermoelasticity. Comput Sci Math Forum. 2023;7:57.
35. Lotfy KH, El-Bary A, Tantawi RS. Effects of variable thermal conductivity of a small semiconductor cavity through the fractional order heat-magneto-photothermal theory. Eur Phys J Plus. 2019;134(6):280. doi:10.1140/epjp/i2019-12631-1.
36. Lotfy KH, Elidy E, Tantawi R. Photothermal excitation process during hyperbolic two-temperature theory for magneto-thermo-elastic semiconducting medium. Silicon. 2021;13:2275–88. doi:10.1007/s12633-020-00795-6.
37. Ailawalia P, Priyanka. Effect of thermal conductivity in a semiconducting medium under modified Green-Lindsay theory. Int J Comput Sci Math. 2024;19(2):167–79. doi:10.1504/IJCSM.2024.137263.
38. Honig G, Hirdes U. A method for the numerical inversion of Laplace Transforms. J Comput Appl Math. 1984;10(1):113–32. doi:10.1016/0377-0427(84)90075-X.
39. Lotfy KH, Elidy E, Tantawi R. Piezo-photo-thermoelasticity transport process for hyperbolic two-temperature theory of semiconductor material. Int J Mod Phys C. 2021;32(7):2150088. doi:10.1142/S0129183121500881.
40. Marin M. Harmonic vibrations in thermoelasticity of microstretch materials. J Vib Acoust Trans ASME. 2010;132(4):44501. doi:10.1115/1.4000971.
41. Mondal S, Sur A. Photo-thermo-elastic wave propagation in an orthotropic se miconductor with a spherical cavity and memory responses. Waves Random Complex Med. 2021;31(6):1835–58. doi:10.1080/17455030.2019.1705426.
42. Bazarra N, Fernández JR, Liverani L, Quintanilla R. Analysis of a thermoelastic problem with the Moore-Gibson–Thompson microtemperatures. J Comput Appl Math. 2024;438:115571. doi:10.1016/j.cam.2023.115571.
43. Ezzat M. A novel model of fractional thermal and plasma transfer within a non-metallic plate. Smart Stru Syst. 2021;27(1):73–87.
44. Kaur I, Kulvinder S, Eduard-Marius C. A mathematical study of a semiconducting thermoelastic rotating solid cylinder with modified Moore-Gibson–Thompson heat transfer under the hall effect. Mathematics. 2022;10(14):2386. doi:10.3390/math10142386.
45. Abouelregal A. Magneto-photothermal interaction in a rotating solid cylinder of semiconductor silicone material with time dependent heat flow. Appl Math Mech. 2021;42(1):39–52. doi:10.1007/s10483-021-2682-6.